2014 International Joint Conference on Neural Networks (IJCNN)
July 6-11, 2014, Beijing, China

Architectural Distortion Detection from Mammograms Using Support Vector Machine

Orawan Netprasat,
Computer Engineering Department,
Faculty of Engineering,
Chiang Mai University,
Chiang Mai, Thailand
orawan.netprasat@gmail.com

Sansanee Auephanwiriyakul*,
Senior Member, IEEE,
Computer Engineering Department,
Faculty of Engineering,
Biomedical Engineering Center,
Chiang Mai University,
Chiang Mai, Thailand
sansanee@ieee.org

Nipon Theera-Umpon,
Senior Member, IEEE,
Electrical Engineering Department,
Faculty of Engineering,
Biomedical Engineering Center,
Chiang Mai University,
Chiang Mai, Thailand
nipon@ieee.org

***Abstract*—One of the leading diseases in women is breast cancer. The detection in an earlier stage is done by indicating the presence of architectural distortion (AD). An AD detection system with support vector machine is developed in this research. The 15 features are extracted from the fuzzy co-occurrence matrix and fractal dimension. The principal component analysis is also implemented to help in feature redundancy reduction. We found out that the best system for the training data set yields 91.67 % correct AD classification with 0.93 sensitivity of detecting AD and 0.91 specificity of detecting true negative. The best result of the blind test mammograms is at 100.00 % correct AD classification with approximately 16 false positive areas per image.**

Keywords—Architectural Distortion; Spiculated Mass; Fuzzy Co-occurrence; Fractal Dimension; Breast Cancer; Support Vector Machine

I. INTRODUCTION

Breast cancer causes a high mortality rate for women and keeps expanding in number. There is no recent discovery of the cause of the disease. To help decrease that rate, earlier detection stage is preferable because the treatment in this stage is more effective. One of important indications is architectural distortion [1]. Architectural distortion that does not result from benign disease, e.g., scar from a surgery, is a disruption of normal arrangement of the breast tissue resulting in a random pattern without an associated mass [1].

There are many research works in breast cancer detection, e.g., [2–4], that do not indicate what kind of breast abnormalities are. Some other works are in the area of mass detection, e.g., [5–8]. The previous mentioned works provide good performance systems, however, it is more useful to identify the type of detected mass. Because the mass type, e.g., architecture distortion, is one of the factors in Breast Imaging-Reporting and Data System (BI-RADS), a quality assurance tool in mammography [1]. Although, there are several research works on architecture distortion (AD) detection [9–12], they often select region of interest (ROI) before hand. There are some other AD detection research works that do not utilize ROI [13, 14], however, the performance is around 70 – 80 %.

In this paper, we develop an AD detection system using support vector machine without any preprocessing phase or ROI selection. In particular, the system can detect AD from other abnormalities, i.e, calcification, circumscribed masses, and spiculated masses.

II. BACKGROUND THEORIES

A. Fuzzy Co-occurrence Matrix

A gray level co-occurrence matrix (GLCM) [15] is a second-order statistic of image. It is constructed by calculating the joint probability of occurrence of two gray values separated by a distance *d*. It is widely used for texture representation. However, in nature, texture might not be precisely repeating and it might have some ambiguity in itself. Hence fuzzy co-occurrence matrix [16, 17] may be another way to incorporate that ambiguity. The fuzzy co-occurrence matrix ($\mathbf{F} = \left[f_{uv}^{d} \right]$, where u and v are the concerned gray values) gives the frequency of occurrence of the fuzzy gray value $\tilde{u}$ followed by a fuzzy gray value $\tilde{v}$ and is defined as [16, 17]

$$f_{uv}^{d} = \sum_{m}\sum_{n}\sum_{\rho}\sum_{k} \min\left(\mu_{\tilde{u}I(m,n)}, \mu_{\tilde{v}I(\rho,k)}\right) \qquad (1)$$

where u and v are all values in the set $\{0,1,\ldots, Lev-1\}$(when Lev is the number of gray level in the image) with the constraint that $|u-v| \geq d$. $I(m,n)$ and $I(\rho,k)$ are the gray values at the pixel (m,n) and (ρ,k), respectively. We set the value of d to 1 for simplicity. $\mu_{\tilde{u}I}$ and $\mu_{\tilde{v}I}$ are symmetric triangular membership functions of crisp number I on the real line and is defined by [16, 17]

$$\mu_{\tilde{u}I} = \max\left(0, 1 - \frac{|I-u|}{\alpha}\right) \quad (2)$$

where u is the crisp counterpart of $\tilde{u}$ and α is a positive real number. At $I = u$, the membership value equals to 1 and the membership function is decreasing to 0 when $(u-I)=\alpha$ and $(I-u)=\alpha$.

We calculated 14 features, i.e., angular second moment, contrast, correlation, variance, inverse difference moment, sum average, sum variance, sum entropy, entropy, difference variance, difference entropy, two information measures of correlation, and maximal correlation coefficient as in [15] but with the fuzzy co-occurrence matrix **F** instead.

B. Fractal Dimension

Fractal dimension is an interesting textural feature. It has been used widely in many pattern recognition applications. Let a self-similar set (A) is a bounded set if A is the union of a number (N_r) of non-overlapping scaled copies of itself where r is the scaling factor [18]. The fractal dimension D of A is

$$D = \frac{\log(N_r)}{\log\left(1/r\right)}. \quad (3)$$

Equation (3) is calculated as in [19, 20], i.e., partitioning an $M \times M$ image into grid of size $s \times s$ where $M/2 \geq s \geq 1$. Hence, $1/r = \left\lfloor M/s \right\rfloor$ [17]. The number of boxes at (i,j) grid [20] is

$$n_r(i,j) = 1 + \sum_{m=1}^{s^2} w(m)\,\mathbf{g}_r(m) \quad (4)$$

where $\mathbf{g}_r(m) = \left[g_r(x_1,y_1), g_r(x_2,y_2), \ldots, g_r\left(x_{s^2}, y_{s^2}\right)\right]$ (5)

and $g_r(x_1,y_1) \leq g_r(x_2,y_2) \leq \ldots \leq g_r\left(x_{s^2}, y_{s^2}\right)$.$w(m)$ is a weight and $g_r(x,y)$ is the gray level of the pixel (x,y) in the (i,j) grid. Please be noted that $\mathbf{g}_r(m)$ in equation (4) is $g_r(x_m,y_m)$. The choice of $w(m)$ [20] is

$$w(m,L,U) = \begin{cases} 1, & \text{if } m = round\left(Us^2\right) \\ -1, & \text{if } m = \max\left(1, round\left(Ls^2\right)\right) \\ 0, & \text{else} \end{cases} \quad (6)$$

where $0 \leq L < U \leq 1$. Since the total number of boxes (N_r) is the summation of the number of boxes ($n_r(i,j)$) in all grids. Then the estimation of N_r is [19, 20]

$$N_r = \sum_{i,j} n_r(i,j). \quad (7)$$

In the experiment, we vary the value of U from 0.55 to 0.95 with step size of 0.05. The value of L is varied from 0.05 to 0.45 with the same step size.

C. Principal Component Analysis

Although, we utilize 14 features from fuzzy co-occurrence matrix and 1 fractal dimension as features to the system, we also try to utilize the principal component analysis (PCA) [21] to reduce the redundancy of these features. Suppose $\mathbf{X} \in \Re^{n \times p}$ contains n samples with p dimensions. The covariance matrix Σ is

$$\Sigma = \mathbf{V}\Lambda\mathbf{V}^t, \quad (8)$$

where $\mathbf{V}$ is an orthogonal matrix with eigenvectors as its column vectors. Λ is a diagonal matrix with the corresponding eigenvalues sorted in ascending order ($\lambda_1 \leq \lambda_2 \leq \ldots \leq \lambda_p$) as its diagonal elements. The transformation matrix $\mathbf{P} \in \Re^{p \times a}$ is used to select a eigenvectors (principal components (PCs)). The cumulative percent variance (CPV) [22, 23] is used to measure the percent variance captured by the first a PCs. The CPV is calculated as

$$\text{CPV}(a) = \frac{\sum_{k=1}^{a} \lambda_k}{trace(\Lambda)} \times 100, \quad \text{for } a \leq p. \quad (9)$$

Then the uncorrelated data set $\mathbf{Y}$ is

$$\mathbf{Y} = \mathbf{XP}. \quad (10)$$

D. Support Vector Machine

We utilize support vector machine [24] as a classifier tool. The radial basis kernel function used in this work is

$$K(\mathbf{x}, \mathbf{x}_i) = \exp\left(-\frac{\|\mathbf{x} - \mathbf{x}_i\|^2}{2\sigma^2}\right). \quad (11)$$

We also utilize a polynomial learning kernel function. This function is defined by

$$K(\mathbf{x}, \mathbf{x}_i) = \left(\mathbf{x}^T \mathbf{x}_i + 1\right)^p. \quad (12)$$

In the experiment, we vary the value of σ from 0.5 to 3.5 with the step size of 0.5. The value of p is varied from 2 to 6 with step size of 1.

III. Experimental Results

We performed the experiment on a standard data set from Mammographic Image Analysis Society (MIAS) [25]. There are 322 mammograms with the size of 1024×1024 containing 7 classes, i.e., architectural distortion (AD), asymmetry (ASYM), calcification (CALC), circumscribed masses (CIRC), other ill-defined masses (MISC), spiculated mass (SPIC), and normal (NORM). In our cases, we did not use mammograms from ASYM and MISC classes because of several varieties of shapes in these 2 classes. Moreover, the number of samples in MISC class is limited. Also, in the real

world diagnosis, it is known that ASYM class is associated with several abnormalities, e.g., AD, CALC, and etc. We selected 71 mammograms, i.e., 42 NORM, 6 CALC, 6 CIRC, 10 AD, and 7 SPIC mammograms to be our training data set. For each mammogram in the training data set, we manually selected an image with the size of 64×64 and collected them in a signature library. Hence we had 42 NORM, 21 CALC, 21 CIRC, 42 AD, and 42 SPIC sub-images in the signature library. Examples of sub-images in the signature library are shown in figure 1. The remaining 222 mammograms, i.e., 163 NORM, 21 CALC, 17 CIRC, 9 AD, and 12 SPIC mammograms wee used as the blind test set.

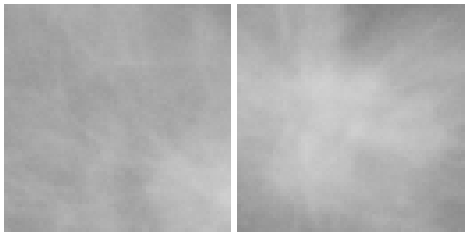

(a) (b)

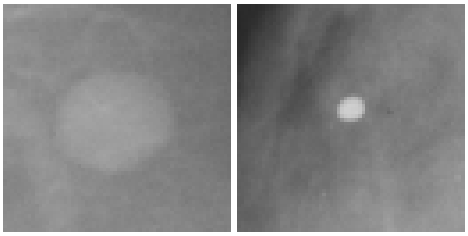

(c) (d)

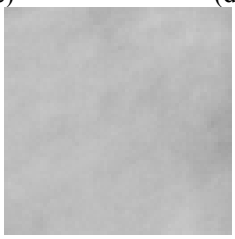

(e)

Fig. 1. Sub-image in the signature library from (a) AD, (b) SPIC, (c) CIRC, (d) CALC, and (e) NORM classes

TABLE I. THE BEST VALIDATION RESULT OF SVM1

Polynomial Kernel (non PCA)									
p	U0.55 L0.45	U0.60 L0.40	U0.65 L0.35	U0.70 L0.30	U0.75 L0.25	U0.80 L0.20	U0.85 L0.15	U0.90 L0.10	U0.95 L0.05
2	82.74	82.74	82.74	82.14	82.74	82.74	83.33	82.74	83.33
3	83.93	84.52	85.71	86.31	85.12	86.31	83.33	83.93	80.95
4	80.95	80.95	82.74	82.14	83.93	83.93	85.71	83.93	83.33
5	77.38	79.17	80.36	80.95	80.36	80.95	80.95	80.36	80.36
6	79.76	76.19	73.81	75.60	77.38	80.36	82.74	80.36	82.14
Polynomial Kernel (PCA)									
p	U0.55 L0.45	U0.60 L0.40	U0.65 L0.35	U0.70 L0.30	U0.75 L0.25	U0.80 L0.20	U0.85 L0.15	U0.90 L0.10	U0.95 L0.05
2	78.57	77.98	82.74	82.74	83.33	83.33	82.14	86.90	85.12
3	82.14	80.36	81.55	82.14	82.14	81.55	80.95	82.74	82.14
4	79.76	32.14	84.52	84.52	82.74	83.93	82.14	80.36	79.17
5	77.98	80.95	82.14	82.74	82.74	83.33	79.76	80.95	79.17
6	76.19	76.19	82.14	87.57	77.98	81.55	79.17	76.79	78.57
RBF Kernel (non-PCA)									
σ	U0.55 L0.45	U0.60 L0.40	U0.65 L0.35	U0.70 L0.30	U0.75 L0.25	U0.80 L0.20	U0.85 L0.15	U0.90 L0.10	U0.95 L0.05
0.5	83.33	85.71	85.71	85.71	85.71	86.90	86.90	86.90	85.12
1	83.93	85.71	86.31	86.31	**89.29**	**89.29**	88.10	86.31	85.12
1.5	83.33	82.74	83.33	83.33	83.33	83.33	83.33	82.74	82.74
2	83.93	82.74	83.33	83.33	83.33	83.33	83.33	82.74	82.74
2.5	81.55	81.55	80.36	80.95	80.95	80.36	80.36	80.36	80.95
3	79.17	78.57	79.17	78.57	78.57	78.57	78.57	79.17	79.17
3.5	78.57	78.57	78.57	78.57	78.57	78.57	78.57	78.57	78.57
RBF Kernel (PCA)									
σ	U0.55 L0.45	U0.60 L0.40	U0.65 L0.35	U0.70 L0.30	U0.75 L0.25	U0.80 L0.20	U0.85 L0.15	U0.90 L0.10	U0.95 L0.05
0.5	71.43	74.40	74.40	75.60	75.00	74.40	76.19	75.00	76.79
1	85.71	85.71	86.31	86.90	86.31	88.10	88.10	88.10	86.31
1.5	84.52	85.71	86.90	86.31	85.12	87.50	86.31	86.90	85.12
2	83.93	84.52	84.52	86.90	83.93	85.12	84.52	85.71	82.74
2.5	83.93	82.74	82.14	82.14	82.74	83.33	82.74	83.93	83.33
3	84.52	82.14	82.14	82.74	82.74	82.74	83.33	83.33	82.74
3.5	80.95	81.55	81.55	80.36	81.55	80.95	81.55	80.36	81.55

The support vector machine (SVM) is known as a binary classifier tool. Since, we would like to detect AD out of the other 4 classes, we trained 2 SVMs to handle multi-class problem. We divided the train data set in the signature library into 2 groups. The first group called ARSP was the combination between AD and SPIC. The other group called OTHER was the combination of the rest 3 classes. We trained the first SVM (SVM1) on the first and second group. We also trained the second SVM (SVM2) with the AD and SPIC training data set. Figure 2 shows the overall system.

In the training process, we utilized leave-one-out cross validation scheme to help the generalization. From the training result of the first SVM shown in table 1, we can see that the feature set from U=0.75, L=0.25 and without PCA trained with SVM with RBF kernel (σ = 1) yields the best validation result , i.e., the correct classification is 89.29% with 0.89 sensitivity of detecting ARSP and 0.89 specificity of detecting true negative. The confusion matrix in this case is shown in table 2. The best validation result of the SVM2 is shown in table 3. We can see that the best result is at 95.24% from 4 models. We manually selected the SVM with RBF kernel (σ = 3) for the feature set from U=0.85, L=0.15 and with PCA out of 4 best models. The confusion matrix of this model is shown in table 4. From the confusion matrix, we can see that this model yields 95.24% correct classification with 0.93 sensitivity of detecting AD, 0.98 specificity of detecting SPIC.

TABLE II. CONFUSION MATRIX OF THE SELECTED MODEL FOR SVM1

		Desired Output	
		ARSP	OTHER
Program class	ARSP	75	9
	OTHER	9	75

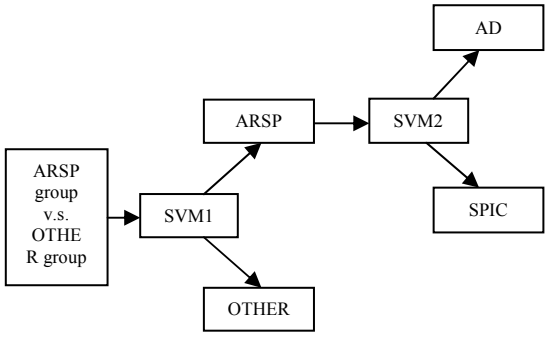

Fig. 2. The SVM model for multi-class problem.

TABLE III. THE BEST VALIDATION RESULT OF SVM2

Polynomial Kernel (non-PCA)									
p	U0.55 L0.45	U0.60 L0.40	U0.65 L0.35	U0.70 L0.30	U0.75 L0.25	U0.80 L0.20	U0.85 L0.15	U0.90 L0.10	U0.95 L0.05
2	89.29	90.48	83.33	84.52	86.90	86.90	88.10	86.90	85.71
3	85.71	88.10	85.71	86.90	85.71	84.52	84.52	89.29	83.33
4	80.95	80.95	82.14	80.95	82.14	83.33	84.52	84.52	83.33
5	82.14	83.33	83.33	82.14	85.71	83.33	88.10	84.52	82.14
6	76.19	79.76	77.38	75.00	73.81	87.57	76.19	76.19	75.00
Polynomial Kernel (PCA)									
p	U0.55 L0.45	U0.60 L0.40	U0.65 L0.35	U0.70 L0.30	U0.75 L0.25	U0.80 L0.20	U0.85 L0.15	U0.90 L0.10	U0.95 L0.05
2	91.67	91.67	86.90	85.71	85.71	86.90	88.10	88.10	88.10
3	86.90	90.48	86.90	88.10	86.90	86.90	84.52	90.48	89.29
4	84.52	85.71	84.52	83.33	84.52	85.71	84.52	83.33	84.52
5	76.19	76.19	75.00	77.38	77.38	77.38	78.57	79.76	79.76
6	72.62	72.62	71.43	72.62	72.62	70.24	71.43	73.81	76.19
RBF Kernel (non-PCA)									
σ	U0.55 L0.45	U0.60 L0.40	U0.65 L0.35	U0.70 L0.30	U0.75 L0.25	U0.80 L0.20	U0.85 L0.15	U0.90 L0.10	U0.95 L0.05
0.5	90.48	90.48	90.48	89.29	88.10	90.48	92.86	91.67	90.48
1	88.10	92.86	85.71	88.10	86.90	89.29	89.29	89.29	89.29
1.5	80.95	80.95	79.76	78.57	78.57	77.38	77.38	72.62	73.81
2	73.81	79.76	73.81	76.19	77.38	76.19	77.38	75.00	72.62
2.5	71.43	76.19	72.62	73.81	77.38	78.57	76.19	73.81	72.62
3	67.86	72.62	67.86	70.24	70.24	72.62	72.62	71.43	72.62
3.5	67.86	71.43	67.86	70.24	70.24	66.67	69.05	69.05	67.86
RBF Kernel (PCA)									
σ	U0.55 L0.45	U0.60 L0.40	U0.65 L0.35	U0.70 L0.30	U0.75 L0.25	U0.80 L0.20	U0.85 L0.15	U0.90 L0.10	U0.95 L0.05
0.5	70.24	66.67	69.05	71.43	69.05	69.05	67.86	66.67	69.05
1	80.95	80.95	80.95	80.95	80.95	88.95	80.95	80.95	80.95
1.5	86.90	88.10	88.10	85.71	86.90	84.52	86.90	85.71	85.71
2	94.05	92.86	91.67	91.67	91.67	92.86	91.67	90.48	90.48
2.5	94.05	94.05	**95.24**	94.05	**95.24**	94.05	**95.24**	94.05	90.48
3	92.86	91.67	91.67	91.67	94.05	94.05	**95.24**	94.05	90.48
3.5	88.10	90.48	90.48	88.10	89.29	89.29	90.48	90.48	89.29

TABLE IV. CONFUSION MATRIX OF THE SELECTED MODEL FOR SVM2

		Desired output	
		AD	SPIC
Program output	AD	39	1
	SPIC	3	41

Once we have SVM1 and SVM2 ready, the system was tested with all of the training data set in the signature library. The confusion of the result of training data set is shown in table 5. We can see that the correct classification rate is 91.67% with 0.93 sensitivity of detecting AD and 0.91 specificity of detecting true negative.

TABLE V. CONFUSION MATIX OF THE TRAINING DATA SET IN THE SIGNATURE LIBRARY

		Desired output		
		AD	SPIC	OTHER
Program output	AD	39	4	6
	SPIC	1	37	0
	OTHER	2	1	78

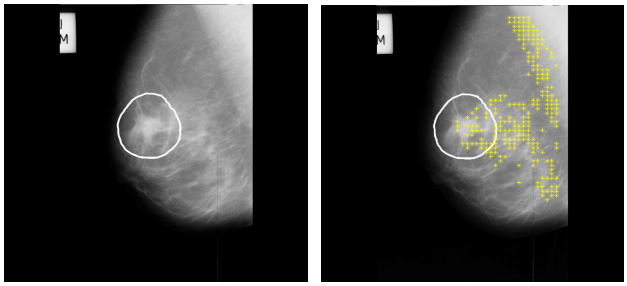

Original

Fig. 3. An example of the successful result from the AD detection system. The expert's opinion (AD area) is shown in circle. The result from the AD detection system is in yellow spots and some spots in the AD area can pass through all threshold values.

We tested the system with the blind test data set. Since, the size of the mammograms were 1024×1024, we scanned 64×64 pixels window with the step size of 16 pixels from top to bottom and left to right in order to generate the 14 features from fuzzy co-occurrence matrix and 1 feature from fractal dimension. These 15 features from U=0.75, L=0.25 and without PCA were used in SVM1. If any area was classified as ARSP, these 15 features from U=0.85, L=0.15 and with PCA would be used in SVM2. The result from both SVM's was put at the center of that window. An example of successful AD detection is shown in figure 3. In this figure, some of the AD detected areas can pass through all threshold values. An example of unsuccessful AD detection is shown in figure 4. If the threshold value is set to 0.95, the system cannot detect the AD area.

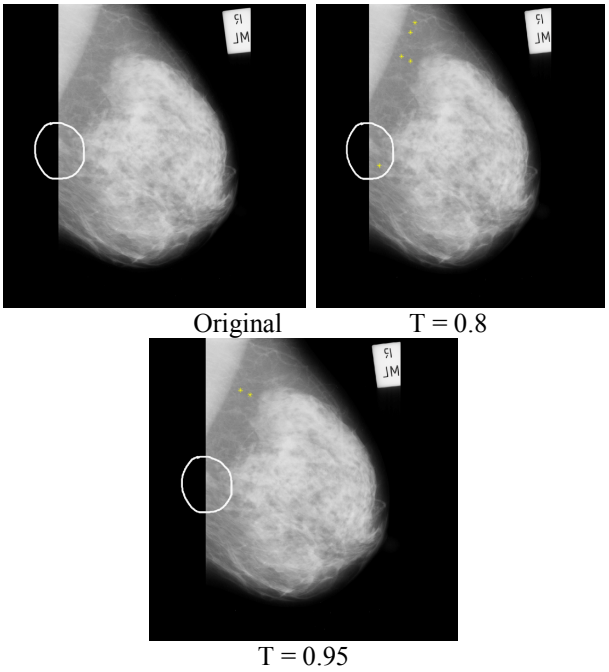

Original T = 0.8

T = 0.95

Fig. 4. An example of the unsuccessful result from the AD detection system. The expert's opinion (AD area) is shown in circle. The result from the AD detection system is in yellow spots and all spots in the AD area cannot pass through if threshold = 0.95.

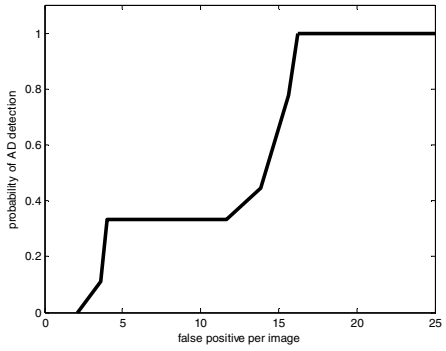

Fig. 5. ROC curve of architectural distortion detection.

To show the ability of the system, we created the receiver operating characteristics (ROC) curve. We counted false positive as one false positive if all pixels are connected as 8-connected component. The ROC curve of the AD detection is shown in figure 5. From the AD detection ROC curve, we can see that the best result is at the threshold = 0.45 with 100% correct AD classification with approximately 16 false positive areas per image. The reason of many false positive areas per image might be because window size of 64×64 is smaller than that of many architectural distortion areas. The system might look at something that is similar to the ones in signature library and classify those areas as AD instead of their corresponding true classes. In addition, we also scan a window with a step of 16, this may make the system miss some points that are important for the classification task.

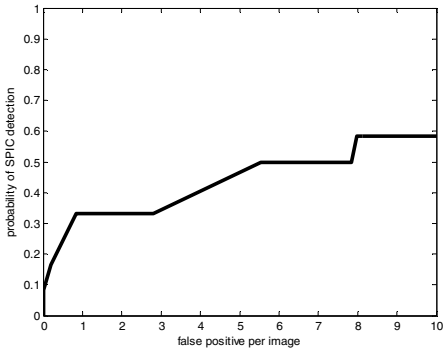

Fig. 6. ROC curve of spiculated mass detection.

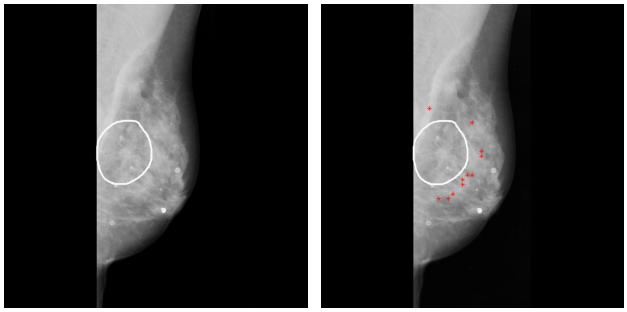

Fig. 7. An example of the unsuccessful result from the SPIC detection system. The expert's opinion (SPIC area) is shown in circle. The result from the SPIC detection system is in red.

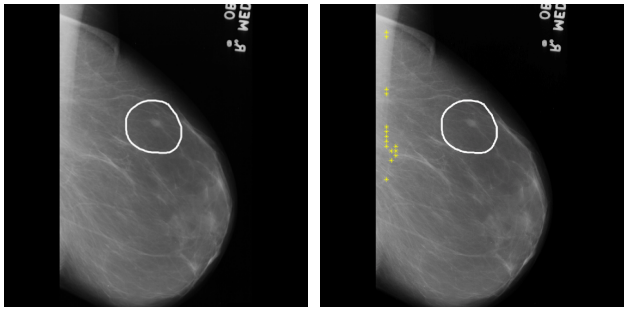

Fig. 8. An example of the unsuccessful result from the SPIC detection system. The expert's opinion (SPIC area) is shown in circle. The result from the AD detection system is in yellow. There is no SPIC detection

Since, there are two types of result from SVM2, i.e., one is for AD and the other is for SPIC. We also plot the ROC curve of SPIC detection as shown in figure 6. We can see that the best detection result is at 58.33% with approximately 8 false positive areas per image. The reason that SPIC detection is not quite good is because sometimes there are calcification areas included in spiculated mass as shown in figure 7. The system will classify them as OTHER class in SVM1 and, hence, they are discarded from SVM2. Sometimes there is no spike boundary around the SPIC areas at all as shown in figure 8. Again, they will be classified by SVM1 as OTHER and are discarded from SVM2. In figure 8, there is no SPIC detection result at all because there is no area similar to SPIC areas in the signature library. Again, scanning a window with a step of 16 may make the system miss some points that are important for the classification task.

IV. Conclusion

In this paper, we develop an architectural distortion (AD) detection system with support vector machine (SVM). We utilize 14 feature set from the fuzzy co-occurrence matrix and another feature from a fractal dimension. We also implement the principal component analysis to reduce a chance of feature redundancy. We found that the best system for the training data set yields 91.67 % correct AD classification with 0.93 sensitivity of detecting AD and 0.91 specificity of detecting true negative. The best result of the blind test mammograms is at 100.00 % correct AD classification with approximately 16 false positive areas per image.

We also report the best blind test mammograms result of the spiculated mass (SPIC) detection. The best result is at 58.33 % with approximately 8 false positive areas per image. This shows that SPIC detection is a more difficult task than AD detection. The reason of difficult SPIC detection is that some SPIC areas are embedded inside calcification area or there is no clear spike boundary.

Acknowledgment

We would like to thank Dr. Pim Handagoon for providing us the breast abnormalities knowledge.

References

[1] M. Muttarak, *Breast Imaging and Intervention*, Chiang Mai University (in Thai).

[2] Y. S. Cho, C. L. Chin, and K. C. Wang, "Based on Fuzzy Linear Discriminant Analysis for Breast Cancer Mammography Analysis," in *2011 International Conference on Technologies and Applications of Artificial Intelligence,* 2011, pp. 57-61.

[3] R. Nithya and B Santhi. Article, "Classification of Normal and Abnormal Patterns in Digital Mammograms for Diagnosis of Breast Cancer," *International Journal of Computer Applications*, vol. 28, no. 6, pp. 21-25, Aug. 2011.

[4] S. Don, D. Chung, K. Revathy, E. Choi, and D. Min, "A New Approach for Mammogram Image Classification Using Fractal Properties," *Cybernetics and Information Technologies*, vol. 12, no. 2, pp. 69-83, Mar. 2013.

[5] S. Auephanwiriyakul, S. Attrapadung, S. Thovutikul, and N. Theera-Umpon, "Breast Abnormality Detection in Mammograms Using Fuzzy Inference System," *2005 IEEE International Conference on Fuzzy Systems*, Reno, Nevada, U.S.A., May 2005, pp.155-160.

[6] D. Cascio, et al., "Mammogram Segmentation by Contour Searching and Mass Lesions Classification With Neural Network," *IEEE Transactions on Nuclear Science*, vol. 53, no. 5, pp. 2827-2833, Oct. 2006.

[7] D.Tralic, J. Bozek, and S. Grgic, "Shape Analysis and Classification of Masses in Mammographic Images Using Neural Networks," in *18th International Conference on Systems, Signals and Image Processing*, 2011, pp. 1-5.

[8] L. O. Martins, G. B. Junior, A. C. Silva, A. C. Paiva, and M. Gattass, "Detection of Masses is Digital Mammograms using K-means and Support Vector Machine", *Electronic Letters on Computer Vision and Image Analysis*, 8(2), 2009, pp. 40 – 50.

[9] A. C. Phadke and P. P. Rage, "Classification of Architectural Distortion from Other Abnormalities in Mammograms," *International Journal of Application or Innovation in Engineering and Management*, vol. 2, pp.42-48, 2013.

[10] Minavathi, S. Murali, M. S. Dinesh, "Model Based Approach for Detection of Architectural Distortions and Spiculated Masses in Mammograms" *International Journal on Computer Science and Engineering,* vol. 3, pp.3534-3545, 2011.

[11] B. Sridhar and K. V. V. S. Reddy, "Architectural Distortion Model for Breast Cancer Detection Based on Mathematical Morphology"

International Journal of Emerging Trends and Technology in Computer Science, vol. 2, issue 2, 2013.

[12] S. Banik, R. M. Rangayyan, and J. E. L. Desautels, "Detection of Architectural Distortion in Prior Mammograms", *IEEE Trans. On Medical Imaging*, vol. 30, no. 2, pp. 279-294, 2011.

[13] M. P. Sampat, G. J. Whitman, M. K. Markey, and A. C. Bovik, "Evidence Based Detection of Spiculated Masses and Architectural Distortions," in *SPIE: Medical Imaging*, vol. 5740, pp. 26-37, Apr. 2005.

[14] T. Ichikawa, T. Matsubara, T. Hara, H. Fujita, T. Endo, and T. Iwase, "Automated Detection Method for Architectural Distortion Areas on Mammograms Based on Morphological Processing and Surface Analysis," in *SPIE: Medical Imaging*, vol. 5370, pp. 920-925, May. 2004.

[15] R. M. Haralick, K. Shanmugam and I. Dinstein, "Textural Features for Image Classification," *IEEE Transactions on Systems, Man and Cybernetics*, vol. 3, no. 6, pp. 610-621, Nov. 1973.

[16] C. V. Jawahar and A. K. Ray, "Fuzzy Statistics of Digital Images", *IEEE Signal Processing Letter*, vol. 3, no. 8, August 1996.

[17] D. Sen and S. K. Pal, "Image Segmentation using Global and Local Fuzzy Statistics," in *2006 Annual IEEE India Conference*, 2006, pp.1-6.

[18] B. B. Mandelbrot, *The Fractal Geometry of Nature*, W.H. Freeman, San Francisco, 1982.

[19] N. Sarkar and B. B. Chaudhuri, "An Efficient Differential Box-Counting Approach to Compute Fractal Dimension of Image," *IEEE Trans. on Systems, Man and Cybernetics*, vol. 24, no. 1, pp. 115-120, Jan. 1994.

[20] N. Theera-Umpon, "Fractal dimension estimation using modified differential box-counting and its application to mstar target classification," in *IEEE International Conference on Systems, Man and Cybernetics*, vol. 2, pp. 537-541, 2002.

[21] D. Garcia-Alvarez, "Fault Detection Using Principal Component Analysis (PCA) in a Wastewater Treatment Plant," in *International Student's Scientific Conference*, pp. 55-59, 2009.

[22] B. Mirmahboub, S. samavi, N. Karimi, and S. Shirani, "Automatic Monocular System for Human Fall Detection Based on Variations in Silhouette Area", *IEEE Transactions on Biomedical Engineering*, vol, 60, no. 2, pp. 427-436, 2013.

[23] E. Auvinet, F. Multon, A. Saint-Arnuad, J. Rousseau, and J. Meunier, "Fall Detection with Multiple Cameras: An Occlusion-resistant Method Based on 3-D Silhouette Vertical Distribution", *IEEE Transactions on Information Technology in Biomedicine,* vol. 15, no. 2, pp. 290-300, March 2011.

[24] C. J. C. Burges, "A Tutorial on Support Vector Machines for Pattern Recognition," *Data Mining and Knowledge Discovery*, vol 2, no. 2, pp. 121-167, 1998.

[25] The Mammographic Images Analysis Society (MIAS): Digital Mammogram Database [Online]. Available: [http://www.mammoimage.org/databases/]